First principles Study of the Reaction of Formic and Acetic Acids with Hydroxyl Radicals

Wenjie Sun and Mark Saeys*

Department of Chemical and Biomolecular Engineering, 4 Engineering Drive 4, National University of Singapore, Singapore 117576

Received: March 7, 2008; Revised Manuscript Received: May 27, 2008

The oxidation of formic and acetic acids with hydroxyl radicals was studied as a model for the oxidation of larger carboxylic acids using first principles calculations. For formic acid, the CBS-QB3 activation barriers of 14.1 and 12.4 kJ/mol for the acid and for the formyl channel, respectively, are within 3 kJ/mol of benchmark W1U values. Tunneling significantly enhances the rate coefficient for the acid channel and is responsible for the dominance of the acid channel at 298 K. At 298 K, tunneling correction factors of 339 and 2.0 were calculated for the acid and the formyl channel using the small-curvature tunneling method and the CBS-QB3 potential energy surface. The Wigner, Eckart, and zero-curvature tunneling methods severely underestimate the importance of tunneling for the acid channel. The resulting reaction rate coefficient of 0.98×10^5 $m^3/(mol \cdot s)$ at 298 K is within a factor 2−3 of experimental values. For acetic acid, an activation barrier of 11.0 kJ/mol and a tunneling correction factor of 199 were calculated for the acid channel. Two mechanisms compete for hydrogen abstraction at the methyl group, with activation barriers of 11.9 and 12.5 kJ/mol and tunneling correction factors of 9.1 and 4.1 at 298 K. The resulting rate coefficient of 1.2×10^5 $m^3/(mol \cdot s)$ at 298 K and branching ratio of 94% compare well with experimental data.

1. Introduction

Carboxylic acids are important constituents in the atmosphere.[1] Formic and acetic acids are the most abundant carboxylic acids in the troposphere with typical concentrations in the parts-per-billion by volume (ppbv) range. They have been detected in vapor and aqueous phases, in particulate matter, and in aerosol particles.[1] In the upper troposphere, carboxylic acids are removed mainly through a free-radical oxidation mechanism initiated by OH• radicals. The initial step of the oxidation mechanism is hydrogen abstraction by OH• radicals. To better understand the lifetime, the degradation pathways, and possible reaction intermediates, accurate kinetic data for the elementary steps in the oxidation reaction are required. However, limited experimental data are available for such reactions and the available data mainly focus on small carboxylic acids. Recently, first principles based procedures have been proposed that can begin to predict reaction rate coefficients for simple hydrogen abstraction reaction with chemical accuracy, i.e., within a factor 2−4 of experimental data.[2–4] To validate the accuracy of first principles based reaction rate calculations for hydrogen abstractions from carboxylic acids by hydroxyl radicals, we have performed benchmark calculations for the reaction rate and for the selectivity between the O−H and the C−H channel for formic and acetic acids.

The reaction of formic acid with OH• radicals has been studied both experimentally[5–9] and theoretically.[10–12] The experimentally reported reaction rate coefficients at 298 K (summarized in Table 3) are fairly consistent and range from $(1.9 \pm 0.1) \times 10^5$ [5] to $(2.95 \pm 0.07) \times 10^5$ $m^3/(mol \cdot s)$,[7] with a recommended value of 2.4×10^5 $m^3/(mol \cdot s)$, obtained by averaging over the available experimental data.[13] The rate coefficient was reported to be relatively temperature independent between 298 and 400 K.[6,8] The reaction of formic acid with OH• radicals can proceed via an acid and a formyl channel (Scheme 1, 1a and 1b), but both lead to the same final products. Because the radical intermediates decompose rapidly to CO_2 and H•, it is difficult to determine the relative rates of channels 1a and 1b. The negligible kinetic isotope effect observed for DCOOH[6,8] indicates that the acid channel (1a) dominates. On the basis of isotope studies, Singleton et al.[8] reported a branching ratio of 91% for the acid channel (1a) at 298 K.

SCHEME 1

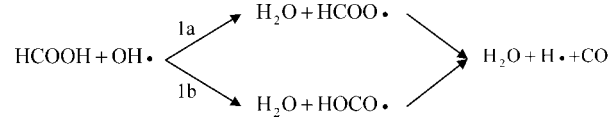

first principles studies of the reaction of formic acid with OH• radicals have been performed by Galano et al.[10] and Anglada.[12] Although both groups report calculated rate coefficients within a factor 2 of experimental data at 298 K, the reported activation energies and pre-exponential factors differ significantly. On the basis of the PMP2/6-311++G(2d,2p)//MP2/6-311++G(2d,2p) level of theory, Galano et al.[10] calculated a zero-point energy inclusive reaction barrier of 28.9 kJ/mol for the dominant acid channel (1a). Anglada[12] reported a significantly lower reaction barrier of 7.8 kJ/mol calculated at the CCSD(T)/aug-cc-pVTZ//QCISD/6-311+G(2df,2p) level of theory. Earlier calculations by the same author[11] for the same geometries but using CCSD(T)/6-311+G(2df,2p) single-point calculations reported a barrier of 13.8 kJ/mol. Anglada noted that this difference "points out the importance of using a flexible basis set in order to obtain a good energetic description".[12] Such a large difference in energy is indeed remarkable, considering that both calculations used polarized triple-ζ basis sets with diffuse functions and basis set superposition corrections were included. Despite the 21 kJ/mol difference in reported activation energies, Galano et al.[10] and Anglada[12] both obtained good agreement with experimental data at 298 K. On the basis of the barrier of 28.9

* Corresponding author. Phone: +65 6516 5826. Fax: +65 6779 1936. E-mail: chesm@nus.edu.sg.

10.1021/jp802017q CCC: $40.75
Published on Web 07/09/2008

SCHEME 2

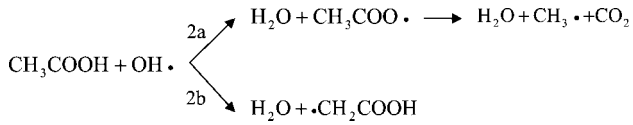

kJ/mol, Galano et al.[10] calculated a tunneling correction factor of 14 252 using the Eckart method.[14] In particular for such large tunneling corrections, the reliability of the Eckart method has been questioned.[15] Consistent with the flatter potential energy surface near the transition state, Anglada calculated a lower tunneling correction factor of 8.5 at 298 K, using the zero-curvature tunneling (ZCT)[16] method.

The oxidation of acetic acid with OH· radicals has also received experimental[5,9,17] and theoretical[18–20] attention. The reported rate coefficients at 298 K range from $(3.6 \pm 0.5) \times 10^{5\ 5}$ to $(5.2 \pm 0.4) \times 10^5$ m^3/(mol·s).[17] The temperature dependence of the reaction rate coefficient has not been conclusively established. Dagaut et al.[9] report an increase of the reaction rate coefficient with temperature between 240 and 440 K, whereas Singleton et al.,[17] Butkovskaya et al.,[21] and Vimal and Stevens[20] observe a decrease over parts of this temperature range. Combining new data with the values reported by Singleton et al.,[17] Butkovskaya et al.[21] proposed a three-parameter expression for the rate coefficient $k = (1.48 \times 10^2$ m^3/(mol·s))$(T/298\ \mathrm{K})^{5.2 \pm 0.7}$ exp[(2400 ± 200) K/T], between 229 and 300 K.

Two channels are available for hydrogen abstraction at acetic acid by OH· radicals (Scheme 2, 2a and 2b). The large kinetic isotope effect of about 4 between CD_3COOH and CD_3COOD indicates that the acid channel (2a) is also the dominant channel for acetic acid oxidation,[17] as confirmed by later studies.[18,21,22] Branching ratios of (64 ± 14)% at 290 K,[18] (64 ± 17)% between 249 and 300 K,[21] and (78 ± 13)% at 298 K[22] have been reported for the acid channel (2a).

first principles calculations for the reaction of acetic acid with OH· radicals confirm that the acid channel is the dominant channel.[18–20] However, to obtain quantitative agreement between reaction rate coefficients calculated at the G2M(CC,MP2) and the G3 levels of theory and experimental values at 298 K, the calculated activation energies needed to be adjusted.[18]

Although first principles calculations have been reported for the reaction of formic acid and OH· radicals, the reported activation energies and tunneling correction factors differ widely. For the reaction of acetic acid with OH· radicals, the agreement between first principles and experimental reaction rate coefficients is less than expected for high-level first principles calculations. In this manuscript, we report benchmark calculations for the reactions between OH· radicals and formic and acetic acids. We show that state-of-the-art first principles calculations are able to predict reaction rate coefficients for this family of reactions with chemical accuracy, i.e., within a factor 4 of experimental values at 298 K, and the selectivity between the acid and the C−H channels can be calculated reliably. In particular, the level of theory required to calculate activation barriers and tunneling factors is addressed. For the reaction between OH· radicals and formic acid, we report calculations at various levels of theory, up to W1U,[23] to reach "benchmark accuracy". Tunneling corrections are calculated on an accurate potential energy surface, using the Wigner, Eckart, and the ZCT methods which consider tunneling along the minimum energy path (MEP) and the small-curvature tunneling (SCT) method which accounts for coupling between the reaction coordinate and the other normal modes. The proposed calculation procedure is then used to study the reaction between acetic acid and OH· radicals.

2. Computational Procedure

Activation energies for the HCOOH + OH· reaction were calculated at several levels of theory. The geometries of reactants, transition states, and products were fully optimized at the B3LYP[24]/cc-pVTZ and the QCISD/6-311++G(d,p) levels of theory. Because the B3LYP method is sometimes considered less accurate for systems containing hydrogen bonds (e.g., ref 25), geometries were also optimized with the computationally more demanding QCISD/6-311++G(d,p) method. Next, single-point energies were calculated for the optimized geometries at different levels of theory. B3LYP/cc-pVTZ was selected as an example of hybrid density functional theory, whereas QCISD/6-311++G(d,p) and CCSD(T)/augh-cc-pVTZ[23] were selected as examples of correlated wave function based methods. The latter basis set was introduced by Martin and de Oliveira for accurate CCSD(T) calculations within the W1 method[23] and corresponds to an aug-cc-pVTZ basis, but without diffuse functions on H atoms. Four higher level compound methods, CBS-QB3,[26] CBS-APNO,[27] Gaussian-3,[28] and W1U (this is the W1 method[23] with UCCSD instead of ROCCSD for open-shell systems) were also employed. For the compound methods, the geometries were constrained at the B3LYP/cc-pVTZ and the QCISD/6-311++G(d,p) optimized structures in the electronic energy calculations. Since the calculations for formic acid indicate that the B3LYP method is suitable for geometry optimizations and the CBS-QB3 method provides accurate energies, these methods were selected to study the CH_3COOH + OH· reaction. All the ab initio calculations were performed with the Gaussian03 computational package.[29]

Tunneling corrections were calculated using the Wigner,[30] Eckart,[14] ZCT,[16] and SCT[31] methods. The Wigner method is a simple, zeroth-order tunneling approximation and only depends on the curvature at the transition state. The Eckart method is believed to be one of the more accurate approximate one-dimensional tunneling corrections.[32] The Eckart tunneling factor is calculated by fitting an Eckart potential to the MEP using the curvature at the transition state, the zero-point energy inclusive energy barrier, and the reaction energy. The tunneling factor, $\kappa(T)$, is then obtained using standard expressions.[14] The ZCT method[16] is a minimum-energy-path, semiclassical adiabatic ground-state (MEPSAG) method which takes into account tunneling along the MEP. Reaction path curvature and coupling to modes orthogonal to the MEP are neglected. The SCT method[31] is a centrifugal-dominant small-curvature semiclassical adiabatic ground-state (CD-SCSAG) method which accounts for the curvature of the reaction path and approximately incorporates tunneling paths other than the MEP. The ZCT and SCT tunneling correction factors were calculated with the Polyrate9.7[33] and the Gaussrate9.7[34] programs.

Tunneling calculations are done on the vibrationally adiabatic ground-state potential energy surface and require an accurate description of the energy variation along the reaction path, in particular near the transition state. Depending on the tunneling approximation, a larger range of the potential energy surface needs to be calculated. Since the CBS-QB3 method was found to provide accurate reaction and activation energies at a reasonable computational cost, this method was selected to calculate the energy change along the MEP, whereas geometries and vibrational frequencies along, and curvatures orthogonal to the MEP were calculated at the B3LYP/6-311G(d,p) level

of theory. This approach is consistent with the approach described by Malick et al.[35] and Saeys et al.[36] A similar method is implemented in the Polyrate9.7 program. The Wigner approximation only requires the curvature along the MEP at the transition state. Consistent with the frequency calculations in the CBS-QB3 method, the curvature was calculated at the B3LYP/6-311G(d,p) level. Though a scaling factor was used for the frequencies that enter the vibrational partition function (see below), no scaling factor was used to calculate the curvature at the transition state. For the Eckart method, the curvature at the transition state was calculated at the B3LYP/6-311G(d,p) level, whereas the energy barrier and the reaction energy are obtained from the CBS-QB3 calculations. The ZCT method requires energies for a larger range of the MEP. The Page−McIver method[37] was used to follow the reaction coordinate. A step size of 0.26 pm was used, and the Hessian was recalculated every nine steps. A smaller step size of 0.026 pm was used near the transition state, for reaction coordinates s between −0.53 and +0.53 pm, where $s = 0$ indicates the transition state at the B3LYP/6-311G(d,p) level of theory. For each of the elementary reactions, a slightly different range of the MEP was mapped, because the location of the reactant and product and the location of the transition state along the MEP at the CBS-QB3 level of theory are slightly different for each of the reactions. For reactions 1a and 1b (Scheme 1), the MEP was calculated from $s = -0.53$ to +0.53 Å, and from $s = -0.79$ to +0.40 Å, respectively. For reactions 2a, 2b1, and 2b2 (Scheme 2 and Figure 5), the MEP was calculated from $s = -0.63$ to +0.79 Å, from $s = -1.06$ to +0.32 Å, and from $s = -1.59$ to +0.37 Å, respectively. For each of the reactions, convergence of the tunneling factor with respect to the range was confirmed. To implement the CBS-QB3 energies along the MEP, the dual-level VTST-ISPE[38] method was used. This is done by providing CBS-QB3 energies for selected points along the MEP. In addition to the energies for the saddle point (s = 0 Å), the reactant and the product, energies at $s = -0.21$, −0.11, +0.05, and +0.21 Å (1a), at $s = -0.26$, +0.10, +0.21, and +0.31 Å (1b), at $s = -0.26$, +0.05, and +0.16 Å (2a), at $s = -0.53$, −0.26, and +0.26 Å (2b1), and at $s = -1.06$, −0.60, −0.31, and +0.37 Å (2b2) were used. Convergence with the number of points was confirmed. The reoriented dividing surface (RODS) algorithm[39] was used to calculate frequencies along the reaction path. Vibrational frequencies at various points along the MEP were calculated in redundant internal coordinates. This was found to improve the continuity of the calculated low frequencies along the reaction coordinate. In addition, low real frequencies were interpolated with the IVTST0FREQ[33] scheme to avoid imaginary frequencies.

Reaction rate coefficients were calculated using the microscopic formulation of transition state theory (TST):

$$k = \kappa(T)\frac{k_B T}{h}\frac{Q_{TS}(T)}{Q_R(T)}e^{\left(\frac{-\Delta E_0(0\,K)}{RT}\right)} \quad (1)$$

where k_B is the Boltzmann constant, h is the Planck constant, $Q_R(T)$ is the reactant partition function, and $Q_{TS}(T)$ is the transition state partition function. $\Delta E_0(0\,K)$ is the energy difference between the transition state and the reactant at 0 K, including the zero-point energy (ZPE). $\kappa(T)$ accounts for tunneling.

Partition functions were calculated using formulas from statistical thermodynamics.[40] Internal rotation partition functions were obtained using the one-dimensional hindered rotation approximation.[41] The rotational potentials were calculated as a function of the torsion angle at 10° intervals using the B3LYP/6-311G(d,p) level of theory. Structures were fully relaxed for each point of the rotational potential, except for rotation around the C(=O)−OH bond in transition state TS2b2 where rotation around the C−C bond was constrained to avoid relaxation to TS2b1 (Figure 5). A 0.9679 scaling factor[42] was used for the frequencies that enter the vibrational partition function. Only the ground state was used to calculate the electronic partition function, except for the hydroxyl radical where the first excited state lies 1.7 kJ/mol above the ground state.[43]

Reactions between carboxylic acids and OH• radicals proceed through a hydrogen-bonded prereactive complex.[7]

SCHEME 3

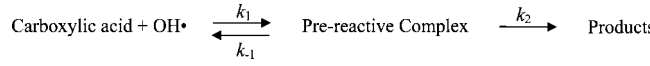

The first step is a reversible, barrierless reaction forming a hydrogen-bonded prereactive complex. The second step is a relatively slow, exothermic hydrogen transfer reaction leading to the products. Within the pseudo-steady-state approximation for the prereactive complex, the overall rate coefficient can be written as

$$k = \frac{k_1 k_2}{k_{-1} + k_2} \quad (2)$$

With the use of collision theory, an upper limit of 5×10^7 m^3/(mol•s) can be estimated for k_1 for the reaction between formic acid and hydroxyl radicals at 298 K. Using a calculated equilibrium constant of 0.26 m^3/mol for the formation of the prereactive complex, a lower limit of 2×10^8 s^{-1} can be obtained for k_{-1}. Since the calculated value for k_2, 9.3×10^5 s^{-1}, is much smaller than the lower limit for k_{-1}, eq 2 can be further simplified using the pseudoequilibrium assumption for the formation of the prereactive complex (eq 3), and the energy of the prereactive complex disappears from the expression for the reaction rate coefficient:

$$k = K_{eq}k_2 = \kappa_2(T)\frac{k_B T}{h}\frac{Q_{TS}(T)}{Q_R(T)}e^{-(E_{TS}-E_R)/RT} \quad (3)$$

where $Q_{TS}(T)$ and E_{TS} are the partition function and the energy at 0 K for the transition state and $Q_R(T)$ and E_R are the partition function and the energy at 0 K for separated reactants. $\kappa_2(T)$ is the tunneling correction factor for the hydrogen transfer reaction.

3. Results and Discussion

The reaction between formic acid and hydroxyl radicals was studied first. Geometries of the reactants, products, transition states, and prereactive complexes were optimized at the B3LYP/cc-pVTZ and QCISD/6-311++G(d,p) levels of theory. The two factors affecting the accuracy of the calculated reaction rate coefficient, i.e., the reaction barrier and the tunneling correction, will be discussed in detail. Next, the reaction between acetic acid and hydroxyl radicals is discussed to validate the accuracy of the recommended procedure for larger carboxylic acids.

3.1. Formic Acid. ***3.1.1. Geometry and Energy Calculations.*** Optimized geometries of reactants, prereactive complexes, transition states, complexes at the product side, and products are shown in Figure 1. Different low-lying electronic states have been reported for the HCOO• radical.[44] The $^2B_2$ state is characterized by symmetric C=O bonds of about 1.25 Å, and an O−C−O angle of 113°, whereas the $^2A_1$ more closely resembles CO_2 and has symmetric C=O bonds of about 1.22

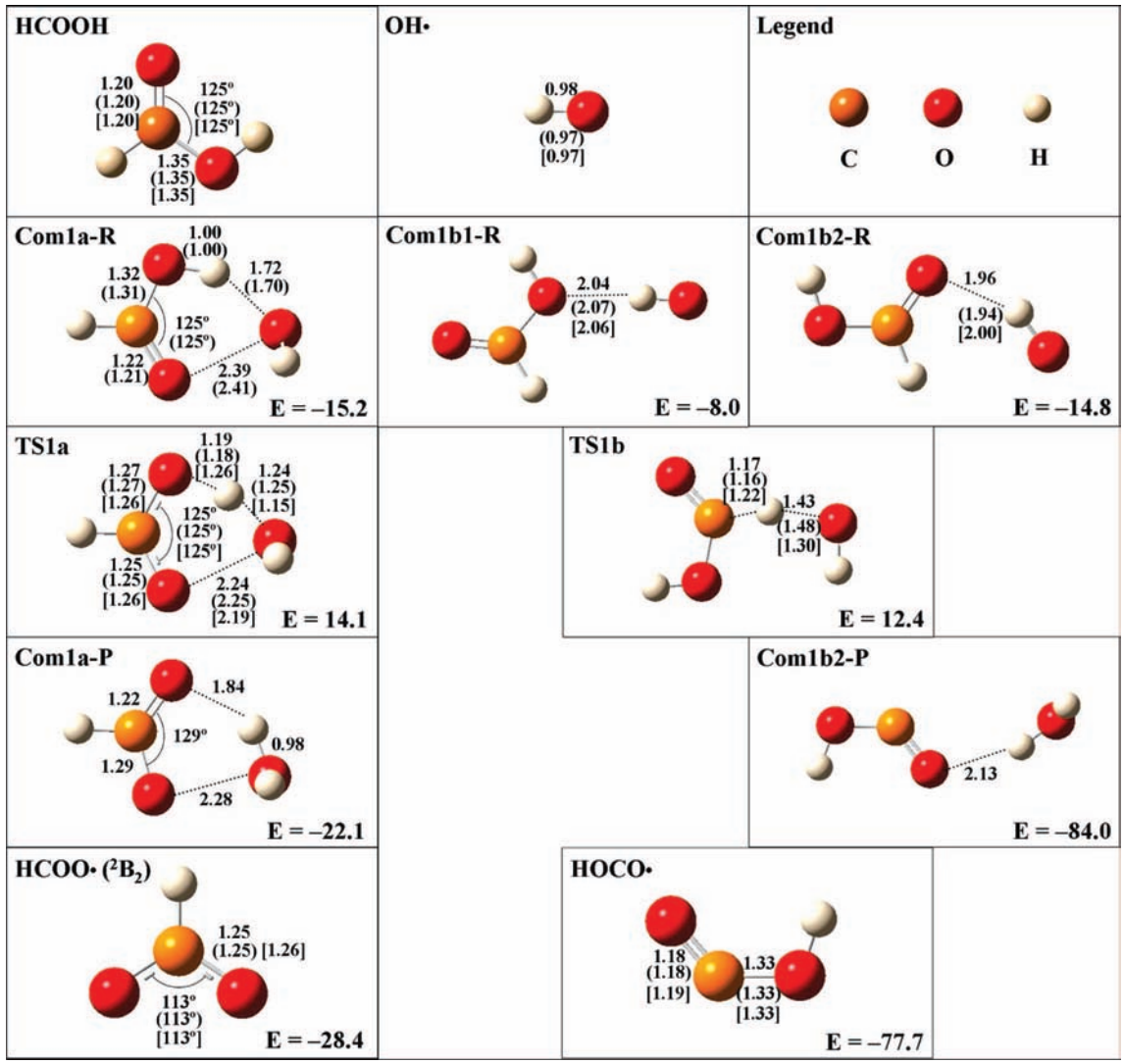

Figure 1. Optimized structures for reactants (HCOOH and OH•), prereactive complexes (Com1a-R, Com1b1-R, and Com1b2-R), transition states (TS1a and TS1b), complexes at the product side (Com1a-P and Com1b2-P), and products (HCOO• and HOCO•) for the reaction between formic acid and a hydroxyl radical. B3LYP/6-311G(d,p) optimized bond lengths (Å) and CBS-QB3 energies at 0 K (kJ/mol, relative to the reactants) are given. The CBS-QB3 energies at 0 K for the products are the reaction energies. B3LYP/cc-pVTZ (round brackets) and QCISD/6-311++G(d,p) (square brackets) optimized bond lengths are also included for the reactants, transition states, prereactive complexes, and products.

Å and an O−C−O angle of 145°. The $^2A'$ state resembles the HCOOH reactant with asymmetric C═O bonds and an O−C−O angle of 123°. The relative stability of the three structures depends on the level of theory, but a benchmark CCSD(T) study by Feller et al.[44] reports that the $^2B_2$ state is 7.9 kJ/mol more stable than the $^2A_1$ state and about 10 kJ/mol more stable than the $^2A'$ state.

It is common to find hydrogen-bonded prereactive complexes for reactions involving hydroxyl radicals.[7,18] Three prereactive complexes are shown in Figure 1. Com1a-R was obtained by following the B3LYP reaction path from the transition state for the acid channel (1a), whereas Com1b1-R and Com1b2-R correspond to the transition state for the formyl channel (1b). Our geometries are similar to the structures reported by Torrent-Sucarrat et al.[45] The stability of the prereactive complex along the acid channel depends on the level of theory. B3LYP calculations lead to Com1a-R. However, this complex is unstable in QCISD calculations, probably due to repulsion between the oxygen lone pairs. A planar prereactive complex characterized by a six-membered ring and two hydrogen bonds was reported by Torrent-Sucarrat et al.[45] and can be obtained following the QCISD reaction path from the transition state. However, at the B3LYP/cc-pVTZ level of theory this complex is a transition state for the internal rotation of the hydroxyl radical and was therefore not included in Figure 1. Note that, following Scheme 3 and eq 3, the prereactive complexes are not kinetically relevant. However, the shape of the energy profile does influence the tunneling factor. Similar hydrogen-bonded complexes were located at the product side. The product complex along the acid channel, Com1a-P, is structurally related to the transition state and to the prereactive complex. Note that the complex corresponds to the $^2A'$ state of the HCOO• radical, not the most stable $^2B_2$ state. At the CBS-QB3 level of theory, the complex is 6.3 kJ/mol less stable than separated H_2O and HCOO• in the $^2B_2$ state but 2.7 kJ/mol more stable than H_2O and HCOO• in the $^2A'$ state.

Two prereactive complexes were optimized for the formyl channel. In Com1b2-R, the hydroxyl radical binds to the more electronegative acyl oxygen, whereas the Com1b1-R complex has a 6.8 kJ/mol weaker hydrogen bond with the hydroxyl oxygen. Both complexes can be found following the B3LYP reaction path from the transition state for the formyl channel,

TABLE 1: Electronic Energies Excluding ZPE (kJ/mol) of the Transition State and the Products, Relative to the Separated Reactants, for the Reaction between Formic Acid and Hydroxyl Radicals

	acid channel, 1a		formyl channel, 1b	
computational method	TS	products	TS	products
B3LYP/cc-pVTZ Geometries				
W1U	11.3	−19.4	13.6	−79.2
CBS-QB3	14.3	−24.8	13.3	−76.8
CBS-APNO	7.9	−26.6	9.5	−79.3
G3	15.9	−21.1	16.3	−74.0
B3LYP/cc-pVTZ	−28.8	−28.1	−9.7	−71.9
QCISD/6-311++G(d,p)	30.6	−4.0	22.6	−64.8
CCSD(T)/augh-cc-pVTZ	11.2	−17.3	14.2	−72.9
QCISD/6-311++G(d,p) Geometries				
CBS-QB3	12.2	−24.9	13.4	−76.8
CBS-APNO	7.2	−26.6	8.8	−79.4
G3	17.2	−21.1	19.9	−74.0
B3LYP/cc-pVTZ	−31.1	−28.0	−11.7	−71.6
QCISD/6-311++G(d,p)	35.1	−4.1	29.9	−65.2
CCSD(T)/augh-cc-pVTZ	9.8	−17.4	16.5	−73.1
Literature Data				
PMP2/6-311++G(2d,2p)//MP2/6-311++G(2d,2p)[a]	34.6		30.9	
QCISD/6-311+G(2df,2p)[b]	29.4			
CCSD(T)/6-311+G(2df,2p)//QCISD/6-311+G(2df,2p)[b]	13.8			
CCSD(T)/aug-cc-pVTZ//QCISD/6-311+G(2df,2p)[c]	7.8		15.4	−73.3

[a] Ref 10. [b] Ref 11. [c] Ref 12.

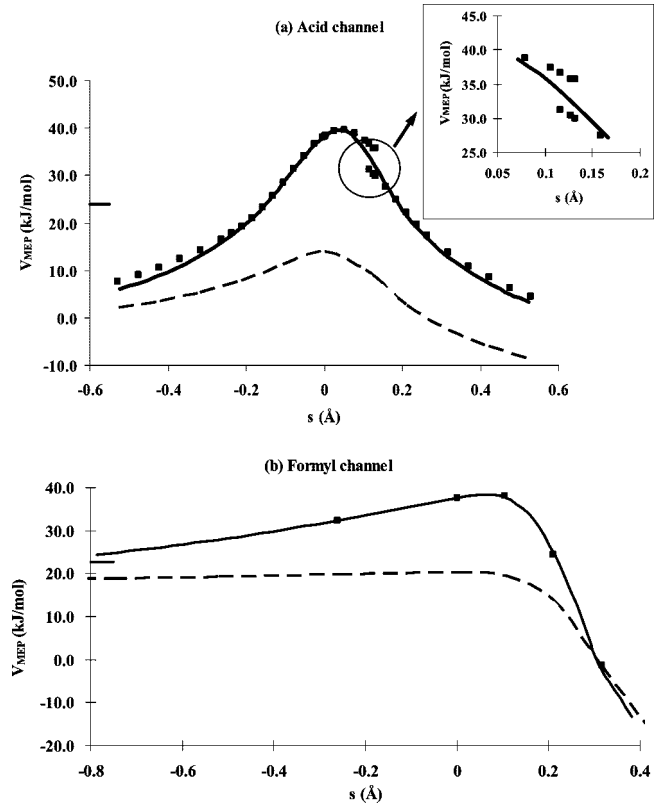

Figure 2. Potential energy profile along the reaction coordinate for the reaction between formic acid and hydroxyl radicals. Electronic energies not including ZPE are relative to the energy of the prereactive complexes, Com1a-R and Com1b2-R. The energies for the separated reactants are indicated by horizontal lines. The inset shows the energy profile near $s = 0.13$ Å. CBS-QB3 values (squares), B3LYP/6-311G(d,p) values (dashed line), and interpolated energy profile used in the Polyrate9.7 calculation (full line).

considering that rotation around the forming H···OH bond is nearly free. Both complexes were also reported by Anglada.[12] The 6.3 kJ/mol hydrogen bond in the product complex Com1b2-P is significantly weaker than the hydrogen bond in the corresponding reactant complex, Com1b2-R. The product complex corresponding to Com1b1-R is not stable at the B3LYP level of theory.

The geometries optimized at the B3LYP/6-311G(d,p) are essentially similar to geometries optimized using a larger cc-pVTZ basis set and fairly similar to the QCISD/6-311++G(d,p) geometries. Increasing the basis set at the B3LYP level of theory changes the bond lengths by an average 0.02 Å and a maximum 0.05 Å. Changing the level of theory to QCISD has little influence on the geometry of the prereactive complexes, Com1b1-R and Com1b2-R, but tends to decrease the forming H···OH bonds by about 0.1 Å and increase the breaking O···H and C···H bonds in the transition states. On the basis of the bond lengths, the B3LYP transition states tend to be earlier than the corresponding QCISD transition states. This is consistent with the reaction barriers in Table 1 (vide infra) and with the structures optimized along the B3LYP MEP. Indeed, the geometries for a reaction coordinate $s = +0.1$ Å are quite similar to the QCISD transition state geometries in Figure 1 for both channels. It is interesting to note that the maxima in CBS-QB3 energy for the geometries along the B3LYP MEP are located at about $s = +0.05$ Å (Figure 2, parts a and b); this is in between the B3LYP and the QCISD transition states.

To evaluate the effect of the difference in geometry on the effective reaction barrier (eq 3) and on the reaction energy, the energy difference between the transition state and the separated reactants and between the reactants and the products was computed at various levels of theory for both geometries (Table 1). The W1U values serve as reference values. This method has a reported mean absolute error of 1.3 kJ/mol for atomization energies for first- and second-row compounds[23] and has been recommended for benchmark accuracy. Both the B3LYP and the QCISD energies deviate significantly from the W1U values. B3LYP calculations significantly overestimate the stability of the transition states, putting them below the level of the separated reactants. Even after correction for the basis set superposition error,[46] the B3LYP/cc-pVTZ transition state energy is still 20.6 kJ/mol below the energy of the separated reactants. Note that this is possible because the prereactive complex, Com1a-R, is even more stable at the B3LYP level. B3LYP overestimates the stability of the HCOO· product and underestimates the stability of the HOCO· product. The low B3LYP reaction barrier is consistent with other benchmark studies.[15,18,47–49] The QCISD method significantly overestimates the height of the reaction barrier and underestimates the exothermicity of both reactions. The high QCISD barriers are also consistent with earlier studies.[11,19] The close agreement between the CCSD(T) and the W1U values, in particular for the reaction barriers, is remarkable, indicating that the CCSD(T) values could be used as a reference as well. The reaction energies differ slightly more. Our W1U and CCSD(T) reaction barriers for the acid channel (1a) are between the values reported by Olivella et al.,[11] 13.8 kJ/mol, and Anglada,[12] 7.8 kJ/mol. For the QCISD transition state geometry, two solutions can be obtained for the HF wave function as illustrated in Figure 2. If we use the unstable, higher energy HF solution as the starting point for the CCSD(T) calculation, a 7.5 kJ/mol barrier is obtained for the acid channel. This value is in better agreement with the value reported by Anglada.[12] The G3 and CBS-QB3 compound method perform quite well. The G3 method tends

to overestimate the reaction barriers by 3−4 kJ/mol, whereas the CBS-QB3 values are slightly closer to the W1U values. Similar accuracy has been reported for the CBS-QB3 and G3 methods for other hydrogen abstraction reactions.[2–4,49] The CBS-QB3 method predicts a slightly lower barrier for the formyl channel by 1.0 kJ/mol, whereas the W1U, CCSD(T), and the G3 methods predict a lower barrier for the acid channel by 2.3, 3.0, and 0.4 kJ/mol, respectively. The similarity between the barriers for both channels is remarkable, considering the much higher stability of the products formed via the formyl channel and the experimentally observed dominance of the acid channel. Clearly, other factors must be responsible for the selectivity of the reaction. The CBS-APNO results are surprisingly far from the W1U values. Similar deviations have been reported for the CBS-APNO method for the hydrogen transfer reaction between H_2O and OH• radicals.[50]

Despite the large differences between the B3LYP and QCISD barriers, single-point CCSD(T) calculations at both geometries give rather similar reaction barriers. Indeed, the barrier for the acid channel decreases by 1.4 kJ/mol, whereas the barrier for the formyl channel increases by 2.3 kJ/mol. The reaction energies remain essentially unchanged. To save CPU time, we did not perform W1U calculations for the QCISD geometry, but we expect the values to be similar to the CCSD(T) results. The trend for the CBS-QB3 energies is similar to the trend for the CCSD(T) energies, whereas the G3 method predicts a slight increase for both barriers when the geometry is modified.

The CBS-QB3 energies at 0 K and relative to the reactants are shown in Figure 1. Since the CBS-QB3 method uses the B3LYP/6-311G(d,p) rather than the B3LYP/cc-pVTZ method for geometry optimization and ZPEs are included in Figure 1, the energies differ slightly from the values in Table 1. Our activation energy of 14.1 kJ/mol for the acid channel is between the barrier of 7.8 kJ/mol reported by Anglada[12] for the CCSD(T)/aug-cc-pVTZ//QCISD/6-311+G(2df,2p) level of theory and the barrier of 28.9 kJ/mol calculated by Galano et al.[10] at the PMP2/6-311++G(2d,2p)//MP2/6-311++G(2d,2p) level of theory. Our activation energy of 12.4 kJ/mol for the formyl channel is slightly higher than the 7.8 kJ/mol barrier calculated by Anglada[12] and significantly lower than the barrier of 23.2 kJ/mol reported by Galano et al.[10]

On the basis of the values in Table 1, we recommend the CBS-QB3 method as a cost-effective method to study hydrogen abstractions at carboxylic acids by hydroxyl radicals. It should be noted that the CBS-QB3 method tends to slightly overestimate the barrier for the acid channel.

3.1.2. Tunneling Corrections. Tunneling can significantly enhance the rate of hydrogen transfer reactions, in particular at low temperatures.[50–52] When tunneling corrections are important, i.e., typically when the tunneling correction factor $\kappa(T)$ is larger than 10, low-order approximations such as the Wigner and the Eckart approximation become less reliable.[15] The ZCT approximation is reliable when most of the tunneling occurs along the reaction coordinate. When the curvature of the MEP becomes important, the system can "cut the corner" in phase space and find a shorter tunneling path inside of the MEP.[31] To account for such tunneling, a larger area of the potential energy surface needs to be characterized. The SCT method is one of the simplest approximations that accounts for reaction-path curvature. It requires the curvatures orthogonal to the reaction coordinate in addition to the potential energy along the MEP. Tunneling corrections were calculated between 200 and 400 K for the acid (1a) and for the formyl (1b) channel, based on the CBS-QB3 energy profile, and using different tunneling approximations, as discussed in section 2. Table 2 summarizes the results.

It can be seen that tunneling corrections for the formyl channel (1b) are rather small. The Wigner and Eckart ap-

TABLE 2: Tunneling Correction Factors for the Reaction between Hydroxyl Radicals and Formic and Acetic Acids for Each Reaction Channel (Figures 1 and 5)

	formic acid		acetic acid		
T (K)	acid	formyl	acid	methyl 2b1	methyl 2b2
			Wigner		
200	4.8	1.1	4.7	3.2	4.5
250	3.5	1.1	3.3	2.4	3.2
298	2.7	1.1	2.6	2.0	2.6
350	2.3	1.0	2.2	1.7	2.1
400	2.0	1.0	1.9	1.5	1.9
1500	1.1	1.0	1.1	1.0	1.1
			Eckart		
200	115	1.1	77	13	101
250	17	1.1	14	4.6	15
298	7.0	1.1	6.1	2.8	5.9
350	4.0	1.0	3.7	2.1	3.4
400	2.8	1.0	2.7	1.8	2.5
1500	1.1	1.0	1.1	1.0	1.1
			Zero-Curvature Tunneling		
200	330	2.6	176	5.7	13
250	47	1.8	31	3.0	5.0
298	16	1.5	12	2.2	3.1
350	7.9	1.4	6.6	1.8	2.3
400	5.0	1.3	4.4	1.5	1.9
1500	1.1	1.0	1.1	1.0	1.0
			Small-Curvature Tunneling		
200	40 700	6.0	13 700	19	104
250	3020	2.8	982	7.0	21
298	339	2.0	199	4.1	9.1
350	93	1.6	62	2.8	5.1
400	39	1.4	28	2.2	3.6
1500	1.4	1.0	1.4	1.1	1.1

TABLE 3: Reaction Rate Coefficients and Branching Ratios at 298 K and 1 atm for the Reaction of Formic and Acetic Acids with Hydroxyl Radicals

HCOOH + OH•				
	rate coefficients (10^5 m^3/(mol•s))			acid channel branching ratio
	acid	formyl	overall	
this work	0.845	0.131	0.977	87%
exptl data			2.41[a]	
			1.9 ± 0.1[b]	
			2.78 ± 0.70[c]	
			2.95 ± 0.07[d]	91%[e]
			2.2 ± 0.2[e]	
			2.23 ± 0.24[f]	
CH_3COOH + OH•				
	rate coefficients (10^5 m^3/(mol•s))			acid channel branching ratio
	acid	methyl	overall	
this work	1.15	0.0766	1.23	94%
exptl data			3.97[g]	
			3.6 ± 0.5[b]	
			4.5 ± 0.4[f]	(78 ± 13)%[i]
			5.2 ± 0.4[h]	

[a] Ref 13. [b] Ref 5. [c] Ref 6. [d] Ref 7. [e] Ref 8. [f] Ref 9. [g] Ref 21. [h] Ref 17. [i] Ref 22.

proximation give similar values, slightly lower than the ZCT method. As explained in section 2, the Wigner and Eckart approximation use the B3LYP curvature at the saddle point to calculate the tunneling correction, whereas the ZCT method uses the CBS-QB3 potential energy surface (Figure 2b). The CBS-QB3 surface is clearly sharper than the B3LYP surface near the transition state, consistent with the underestimation of the reaction barrier by the B3LYP method (Table 1). The low second derivative at the transition state calculated by the B3LYP method leads to a fairly wide Eckart potential barrier and hence a low tunneling probability. The reaction-path curvature along the MEP is fairly important, and the SCT correction is about a factor 2 higher than the ZCT correction at 200 K.

The reaction rate coefficient for the acid channel is significantly enhanced by tunneling. The Wigner and Eckart method underestimate the tunneling correction as compared to the ZCT method. This can again be related to the underestimation of the curvature at the transition state by the B3LYP method. Figure 2a shows the CBS-QB3 and the B3LYP potential energy profiles (V_{MEP}) along the reaction coordinate. Note that the transition state along the CBS-QB3 energy profile is located at $s = 0.05$ Å and is, hence, slightly later than the B3LYP transition state. This is consistent with the earlier discussion of Table 1. The CBS-QB3 profile shows a small discontinuity around $s = +0.13$ Å. Two low-lying solutions can be obtained for the HF wave function for geometries near $s = 0.13$ Å. Each solution leads to a slightly different CBS-QB3 energy, and both values are shown in the inset of Figure 2a. To evaluate the reliability of the CBS-QB3 energies for geometries near $s = 0.13$ Å, the T_1 diagnostic was used.[53] For open-shell systems, a T_1 diagnostic above 0.044 has been proposed as an indication that multireference methods should be used.[54] Our value of 0.025 is well below this number, and single-reference methods such as the CBS-QB3 method can be used. Note that the discontinuity occurs well beyond the transition state, and only one HF solution dominates near the transition state. For the dual-level tunneling calculations (section 2), CBS-QB3 energies at $s = -0.21$, -0.11, 0.0, $+0.05$, and $+0.21$ Å were used. A single HF solution dominates for those points. For the acid channel, the tunneling correction increases by a factor 123 at 200 K and by a factor 21 at 298 K when the reaction-path curvature is included using the SCT method. When the reaction-path curvature is very large, the SCT approximation tends to underestimate the tunneling probability,[55] and the actual tunneling correction might be even larger than the values in Table 2. To accurately account for tunneling paths outside the MEP region we would need to go beyond the SCT approximation and explore a larger area of the potential energy surface. The curvature along the reaction path for the acid channel is shown in Figure 3a. High curvatures are found at $s = -0.14$ and $+0.21$ Å. Analysis of the SCT calculations indicates that certain vibration modes couple with the reaction coordinate. Both peaks are mainly due to coupling between the reaction coordinate and the H−O−H bending modes. Strong reaction-path curvature coupling leads to a low reduced effective mass and increases the tunneling probability.[55] The strong coupling is probably caused by the compact nature of the reaction center in hydrogen transfer reactions between the acid OH group in carboxylic acids and the attacking hydroxyl radical (Figure 1, TS1a).

On the basis of the above results, the SCT approach is required to begin to calculate accurate tunneling correction factors for the acid channel. Methods that do not account for reaction-path curvature such as the Wigner, Eckart, and ZCT method significantly underestimate the contribution of tunneling

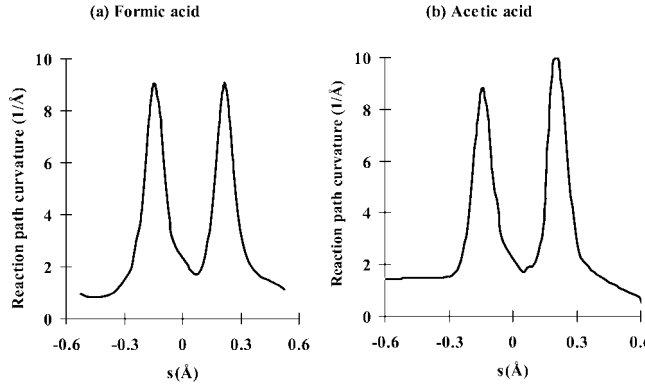

Figure 3. Reaction-path curvature along the acid channel reaction path for the reactions of formic and acetic acids with hydroxyl radicals.

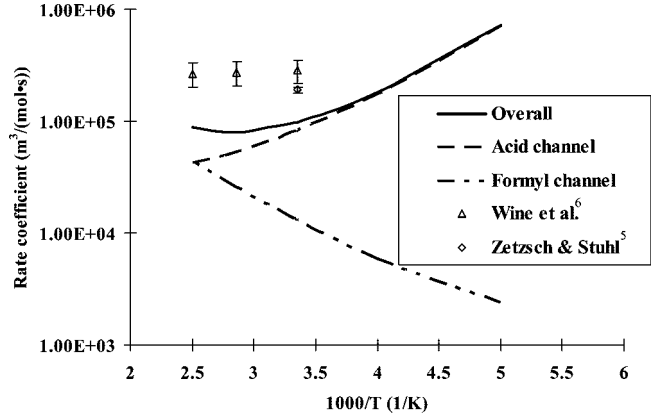

Figure 4. Arrhenius plot of the overall reaction rate coefficient and for each of the reaction channels for the reaction between formic acid and hydroxyl radicals.

to the reaction rate coefficient for the acid channel at ambient conditions. The high tunneling factor is responsible for the dominance of the acid channel at 298 K.

3.1.3. Rate Coefficient and Selectivity. The SCT tunneling correction factors (Table 2) were combined with partition functions calculated following the procedures outlined in section 2 and the CBS-QB3 activation energies (Figure 1) to obtain rate coefficients for both channels. The rate coefficients and branching ratios are compared with available experimental values in Table 3 and in Figure 4. The calculated rate coefficient at 298 K for the overall reaction is a factor 2−3 lower than the range of reported experimental values. Such agreement is remarkable, considering that a 2 kJ/mol decrease in the activation energy increases the rate coefficient at 298 K by a factor 2.2. The data in Table 1 indicate that the CBS-QB3 method predicts a slightly higher barrier than the W1U method for the dominant acid channel. In addition, the SCT method might underestimate the tunneling correction when the reaction-path curvature is large.[55] Both considerations are consistent with the underestimation of the experimental rate coefficient. At 298 K, 87% of the overall reaction was found to proceed through the acid channel (1a). This value is in agreement with the experimental value of 91%, estimated by Singleton et al.[8] using isotopic-labeling experiments.

An Arrhenius plot of the rate coefficients between 200 and 400 K is shown in Figure 4. The rate coefficient for the acid channel decreases with increasing temperature, whereas the rate coefficient of the formyl channel increases. The decrease of the rate coefficient for the acid channel with temperature for low temperatures is caused by the rapid decrease of the tunneling

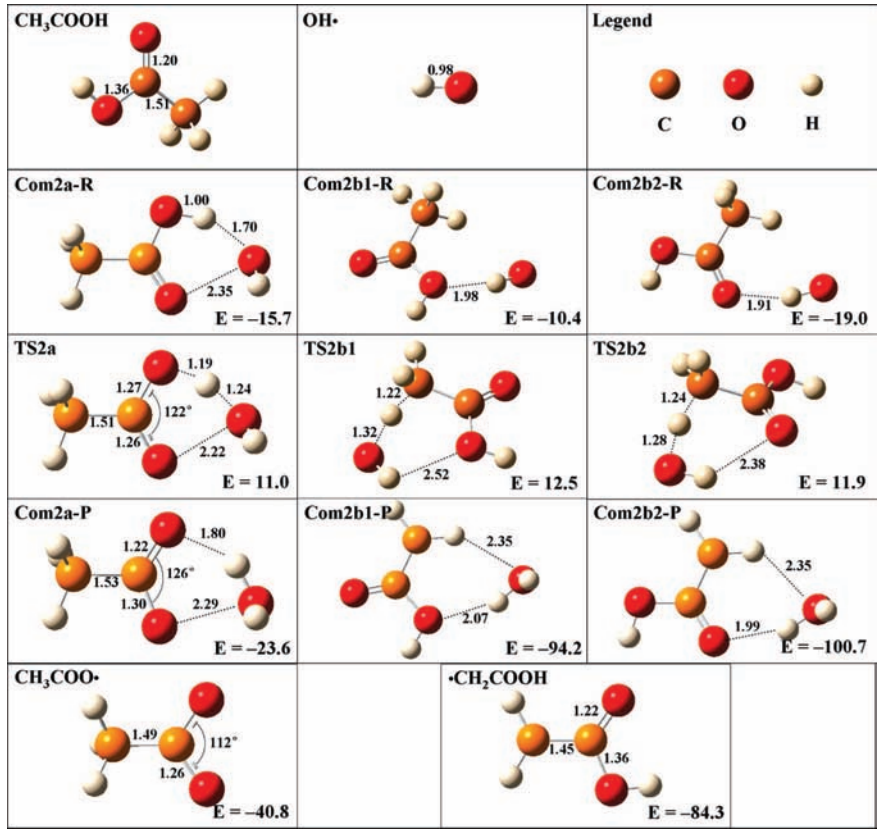

Figure 5. Optimized structures for the reactants (CH_3COOH and OH•), prereactive complexes (Com2a-R, Com2b1-R, and Com2b2-R), transition states (TS2a, TS2b1, and TS2b2), complexes at the product side (Com2a-P, Com2b1-P, and Com2b2-P), and products (CH_3COO• and •CH_2COOH) for the reaction between acetic acid and a hydroxyl radical. B3LYP/6-311G(d,p) optimized bond lengths (Å) and CBS-QB3 energies at 0 K (kJ/mol, relative to the reactants) are given. The CBS-QB3 energies at 0 K for the products (CH_3COO• and •CH_2COOH) are the reaction energies.

factor with temperature and not by a negative effective activation barrier. The overall rate coefficient decreases slightly with temperature below 350 K, whereas it increases with temperature above 350 K. The resulting temperature independence of the overall rate coefficient between 298 and 400 K is consistent with the experimental data reported by Wine et al.[6]

3.2. Acetic acid. ***3.2.1. Geometry and Energy Calculations.*** In this section, we apply the recommended procedure developed in the previous section to the reaction between acetic acid and hydroxyl radicals. Optimized geometries of reactants, prereactive complexes, transition states, complexes at the product side, and products are shown in Figure 5. Three prereactive complexes were again located. The geometries and energies of the complexes (Com2a-R and Com2a-P) and the transition state (TS2a) for the acid channel (2a) are similar to the corresponding structures for formic acid (Figure 1). They are also similar to structures optimized at the B3LYP/6-311++G(2df,2pd) level of theory by De Smedt et al.[18] The structures of the prereactive complexes for the methyl channel are also similar to formic acid, though the complexes with acetic acid are slightly more stable due to the higher electron density on the oxygen atoms of acetic acid. Because a hydrogen bond is maintained in the transition state for the methyl channel, two different transition states are identified for the methyl channel. For the reaction with formic acid, a similar hydrogen bond is not observed, and rotation around the forming H···OH bond is nearly free in the transition state for formic acid. The transition states for the methyl channel (2b) differ slightly from the structure reported by De Smedt et al.[18] but are similar to the structures proposed by Rosado-Reyes and Francisco.[19] The product complexes are characterized by two hydrogen bonds, and they are about 10 kJ/mol more stable than the corresponding product complex for formic acid. Because the hydrogen bond with the C−OH group in Com2b1-P is fairly weak at 9.9 kJ/mol, it is not surprising that the corresponding complex could not be optimized for formic acid.

Low-lying electronic states can again be identified for the CH_3COO• radical. At the CBS-QB3 level, the most stable state is the $^2A''$ state. This state is electronically and structurally similar to the $^2B_2$ state for the HCOO• radical. The $^2A'$ state in CH_3COO• is related to the $^2A'$ state in the HCOO• radical and is 24.5 kJ/mol less stable than the $^2A''$ state at the CBS-QB3 level. The acid channel in acetic acid is 12.4 kJ/mol more exothermic than in formic acid. Analysis of the calculations indicates that the methyl group stabilizes COO• group in the product. Indeed, increasing the CH_3−COOH bond length by up to 0.4 Å in the calculations reduces the calculated exothermicity, whereas increasing the H−COOH bond length increases the exothermicity for formic acid. The transition state and the product complex, Com2a-P, for the acid channel are structurally related to the $^2A'$ state, and the complex is less stable than the separated CH_3COO• ($^2A''$) radical and a H_2O molecule. The effective reaction barrier for the acid channel, 11.0 kJ/mol, is between the values reported by De Smedt et al.,[18] i.e., 13.8 kJ/mol using G2M(CC,MP2)//MP2/6-311++G(2df,2pd) and 6.7 kJ/mol using G2M(CC,MP2)//B3LYP/6-311++G(2df,2pd), and 3.1 kJ/mol lower than the barrier for the acid channel in formic acid.

The methyl channel is 43.5 kJ/mol more exothermic than the acid channel and 6.6 kJ/mol more favorable than the formyl channel in formic acid. It is also 8.8 kJ/mol more exothermic than the corresponding reaction between ethane and OH• at the

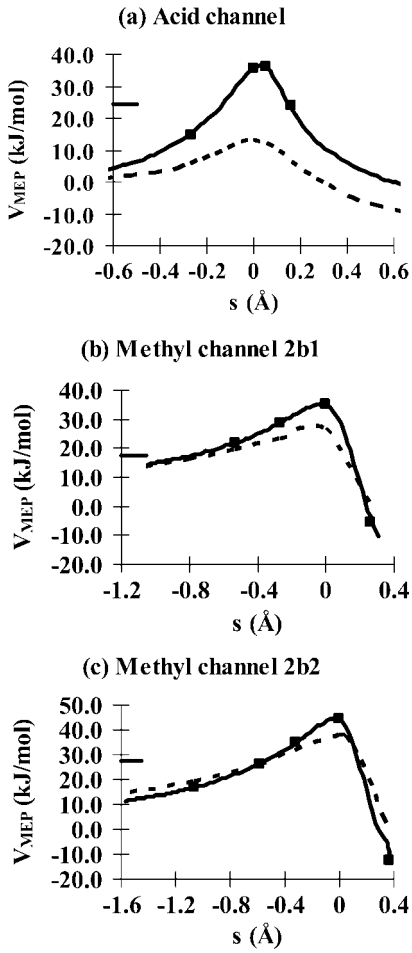

Figure 6. Potential energy profiles along the reaction coordinate for the reaction between acetic acid and hydroxyl radicals. Electronic energies not including the ZPE are relative to the energy of the prereactive complexes. Reactant energies are indicated by horizontal lines. CBS-QB3 values used for fitting (squares), B3LYP/6-311G(d,p) values (dashed line), and interpolated energy profile used in the Polyrate9.7 calculation (full line).

same level of theory. The effective barriers for the two methyl channels, 11.9 and 12.5 kJ/mol, are comparable to the barrier for the formyl channel, 12.4 kJ/mol, and slightly higher than the barrier for the reaction between a hydroxyl radical and ethane, 9.3 kJ/mol. The barriers for the methyl and the acid channel are again very similar, differing less than 1.5 kJ/mol. The small difference indicates that the reaction barriers are not responsible for the observed dominance of the acid channel. De Smedt et al.[18] reported a 4.8 kJ/mol higher barrier for the methyl channel, leading to a 8.8 kJ/mol difference between the methyl and the acid channel.

3.2.2. Tunneling Corrections. Tunneling corrections were calculated using the Wigner, Eckart, ZCT, and SCT methods and are summarized in Table 2. The potential energy surfaces for the acid and both methyl channels are shown in Figure 6. Tunneling is again very important for the acid channel and is caused by the strong reaction-path curvature at $s = -0.14$ Å and at $s = +0.21$ Å (Figure 3b), with reaction-path curvature couplings of 3.8 and 2.6 Å^{-1} at $s = -0.14$ Å, and 6.0 and 6.8 Å^{-1} at $s = 0.21$ Å for two H−O−H bending modes. The tunneling correction for the acid channel in acetic acid is a factor 2−3 smaller than for the acid channel in formic acid. This can be related to the lower barrier and the slightly flatter potential energy surface for acetic acid. The B3LYP potential energy surface is again flatter than the CBS-QB3 surface, leading to low Wigner and Eckart tunneling factors. Tunneling factors for the methyl channel are significantly larger than for the formyl channel. Coupling between the reaction coordinate and other normal modes also increases tunneling for the methyl channels, and the SCT tunneling factors are a factor 2−7 larger than the ZCT factors. The maximum curvature coupling for the methyl reaction paths, 6.0 Å^{-1} at $s = -0.12$ Å, is larger than the maximum curvature coupling of the formyl reaction path, 1.6 Å^{-1} at $s = -0.36$ Å. The more compact nature of the transition state for acetic acid, TS2b1 and TS2b2, caused by a hydrogen bond between acetic acid and the hydroxyl radical is probably responsible for the higher reaction-path curvature coupling. The Eckart method predicts tunneling factors within a factor 2 of the more expensive SCT method for the methyl channels and might be used as a cost-effective method for reactions between a methyl group and a hydroxyl radical. However, the agreement is partly due to a cancellation of errors. The Eckart potential is narrower than the CBS-QB3 potential energy surface (Figure 6c), leading to an overestimation of the tunneling factor, e.g., compared to the ZCT value. However, coupling between the reaction coordinate and the other normal modes is neglected in the Eckart method, leading to an underestimation of the tunneling factor.

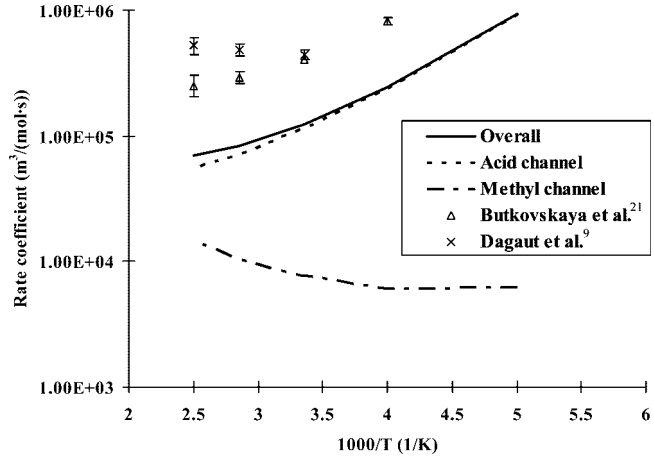

Figure 7. Arrhenius plot of the overall reaction rate coefficient and for each of the reaction channels for the reaction between acetic acid and hydroxyl radicals.

3.2.3. Rate Coefficient and Mechanism. The SCT tunneling factors (Table 2) were combined with partition functions calculated following the procedures outlined in section 2 and the CBS-QB3 activation energies (Figure 5) to obtain rate coefficients for both channels. The rate coefficients and branching ratios are compared with available experimental values in Table 3 and in Figure 7. The calculated overall rate coefficient is a factor 3−4 smaller than the experimental data and 26% larger than the calculated rate coefficient for formic acid. Experimentally, the rate coefficient for acetic acid is about 65% higher than the rate coefficient for formic acid. Considering the tendency of the CBS-QB3 method to slightly overestimate the reaction barrier for the acid channel (by about 2−3 kJ/mol, Table 1) and the importance of tunneling for both channels in acetic acid, the agreement is promising. The slightly low value for the acetic acid reaction rate coefficient might in part be due to an underestimation of the importance of tunneling for the methyl channel. Though the SCT tunneling factor is a factor 3 smaller for the acid channel in acetic acid, the effective activation barrier is 3.1 kJ/mol lower, and the resulting rate coefficients at 298 K are similar for both acids. Below 400 K the acid channel is the dominant channel, and the calculated branching ratio at 298 K

of 94% is at the top range of the experimental values, 78% ± 13%. The overall rate coefficient is calculated to decrease with temperature, consistent with the trend reported by Butkovskaya et al.[21]

4. Conclusion

The reaction between hydroxyl radicals and formic and acetic acids was studied using high-level quantum chemical calculations. The effects of the level of theory on the activation energy and on the tunneling factor were examined in detail. The overall reaction rate coefficient and the selectivity between the acid and the C−H channels were discussed. For formic acid, effective activation barriers of 14.1 and 12.4 kJ/mol were calculated with the CBS-QB3 method for the acid and the formyl channel, respectively. The CBS-QB3 barriers are within 3 kJ/mol of reference W1U and large basis set CCSD(T) values. Tunneling was found to significantly enhance the rate coefficient for the acid channel, with an SCT correction factor of 339 at 298 K, calculated for the CBS-QB3 potential energy surface. Tunneling approximations that do not account for the reaction-path curvature coupling significantly underestimate the importance of tunneling for the acid channel. The calculated overall rate coefficient at 298 K, 0.98×10^5 m^3/(mol•s), is within a factor 2−3 of experimental values.

For the dominant acid channel in acetic acid, the lower barrier of 11.0 kJ/mol and the lower SCT tunneling correction of 199 lead to a rate coefficient at 298 K for the acid channel that is 30% higher than for formic acid. Two reaction paths are available for hydrogen abstraction at the methyl group in acetic acid. The effective barriers of 11.9 and 12.5 kJ/mol are similar to the barrier for the formyl channel in formic acid. The more compact nature of the transition states leads to higher reaction-path curvatures and higher tunneling correction factors of 9 and 4 at 298 K. The resulting overall rate coefficient at 298 K, 1.2×10^5 m^3/(mol•s), is within a factor 3−4 of experimental values.

Acknowledgment. We acknowledge the National University of Singapore (NUS) for funding. The authors thank Liming Yang and Liya Yu for fruitful discussions.

References and Notes

(1) Chebbi, A.; Carlier, P. *Atmos. Environ.* **1996**, *30*, 4233–4249.
(2) Ellingson, B. A.; Truhlar, D. G. *J. Am. Chem. Soc.* **2007**, *129*, 12765–12771.
(3) Saeys, M.; Reyniers, M. F.; Van Speybroeck, V.; Waroquier, M.; Marin, G. B. *ChemPhysChem* **2006**, *7*, 188–199.
(4) Hemelsoet, K.; Moran, D.; Van Speybroeck, V.; Waroquier, M.; Radom, L. *J. Phys. Chem. A* **2006**, *110*, 8942–8951.
(5) Zetzsch, C.; Stuhl, F. *Physico-Chemical Behavior of Atmospheric Pollutants. Proceedings of the Second European Symposium*; D. Reidel: Dordrecht, The Netherlands,1982; pp 129−137.
(6) Wine, P. H.; Astalos, R. J.; Mauldin, R. L., III *J. Phys. Chem.* **1985**, *89*, 2620–2624.
(7) Jolly, G. S.; McKenney, D. J.; Singleton, D. L.; Paraskevopoulos, G.; Bossard, A. R. *J. Phys. Chem.* **1986**, *90*, 6557–6562.
(8) Singleton, D. L.; Paraskevopoulos, G.; Irwin, R. S.; Jolly, G. S.; McKenney, D. J. *J. Am. Chem. Soc.* **1988**, *110*, 7786–7790.
(9) Dagaut, P.; Wallington, T. J.; Liu, R.; Kurylo, M. J. *Int. J. Chem. Kinet.* **1988**, *20*, 331–338.
(10) Galano, A.; Alvarez-Idaboy, J. R.; Ruiz-Santoyo, M. E.; Vivier-Bunge, A. *J. Phys. Chem. A* **2002**, *106*, 9520–9528.
(11) Olivella, S.; Anglada, J. M.; Solé, A.; Bofill, J. M. *Chem. Eur. J.* **2004**, *10*, 3404–3410.
(12) Anglada, J. M. *J. Am. Chem. Soc.* **2004**, *126*, 9809–9820.
(13) Sander, S. P.; Friedl, R. R.; Golden, D. M.; Kurylo, M. J.; Huie, R. E.; Orkin, V. L.; Moortgat, G. K.; Ravishankara, A. R.; Kolb, C. E.; Molina, M. J.; Finlayson-Pitts, B. J. *Chemical Kinetics and Photochemical Data for Use in Atmospheric Studies*; Evaluation No. 14; JPL Publication 02-25; JPL: Pasadena, CA, 2003.
(14) Eckart, C. *Phys. Rev.* **1930**, *35*, 1303–1309.
(15) Kuwata, K. T.; Dibble, T. S.; Sliz, E.; Petersen, E. B. *J. Phys. Chem. A* **2007**, *111*, 5032–5042.
(16) Garrett, B. C.; Truhlar, D. G.; Grev, R. S.; Magnuson, A. W. *J. Phys. Chem.* **1980**, *84*, 1730–1748.
(17) Singleton, D. L.; Paraskevopoulos, G.; Irwin, R. S. *J. Am. Chem. Soc.* **1989**, *111*, 5248–5251.
(18) De Smedt, F.; Bui, X. V.; Nguyen, T. L.; Peeters, J.; Vereecken, L. *J. Phys. Chem. A* **2005**, *109*, 2401–2409.
(19) Rosado-Reyes, C. M.; Francisco, J. S. *J. Phys. Chem. A* **2006**, *110*, 4419–4433.
(20) Vimal, D.; Stevens, P. S. *J. Phys. Chem. A* **2006**, *110*, 11509–11516.
(21) Butkovskaya, N. I.; Kukui, A.; Pouvesle, N.; Le Bras, G. *J. Phys. Chem. A* **2004**, *108*, 7021–7026.
(22) Crunaire, S.; Tarmoul, J.; Fittschen, C.; Tomas, A.; Lemoine, B.; Coddeville, P. *Appl. Phys. B: Lasers Opt.* **2006**, *85*, 467–476.
(23) Martin, J. M. L.; de Oliveira, G. *J. Chem. Phys.* **1999**, *111*, 1843–1856.
(24) Stephens, P. J.; Devlin, F. J.; Chabalowski, C. F.; Frisch, M. J. *J. Phys. Chem.* **1994**, *98*, 11623–11627.
(25) Xu, X.; Zhang, Q. S.; Muller, R. P.; Goddard, W. A., III *J. Chem. Phys.* **2005**, *122*, 014105.
(26) Montgomery, J. A., Jr.; Frisch, M. J.; Ochterski, J. W.; Petersson, G. A. *J. Chem. Phys.* **1999**, *110*, 2822–2827.
(27) Ochterski, J. W.; Petersson, G. A.; Montgomery, J. A., Jr. *J. Chem. Phys.* **1996**, *104*, 2598–2619.
(28) Curtiss, L. A.; Raghavachari, K.; Redfern, P. C.; Rassolov, V.; Pople, J. A. *J. Chem. Phys.* **1998**, *109*, 7764–7776.
(29) Frisch, M. J.; Trucks, G. W.; Schlegel, H. B.; Scuseria, G. E.; Robb, M. A.; Cheeseman, J. R.; Montgomery, J. A., Jr.; Vreven, T.; Kudin, K. N.; Burant, J. C.; Millam, J. M.; Iyengar, S. S.; Tomasi, J.; Barone, V.; Mennucci, B.; Cossi, M.; Scalmani, G.; Rega, N.; Petersson, G. A.; Nakatsuji, H.; Hada, M.; Ehara, M.; Toyota, K.; Fukuda, R.; Hasegawa, J.; Ishida, M.; Nakajima, T.; Honda, Y.; Kitao, O.; Nakai, H.; Klene, M.; Li, X.; Knox, J. E.; Hratchian, H. P.; Cross, J. B.; Bakken, V.; Adamo, C.; Jaramillo, J.; Gomperts, R.; Stratmann, R. E. ; Yazyev, O.; Austin, A. J.; Cammi, R.; Pomelli, C.; Ochterski, J. W.; Ayala, P. Y.; Morokuma, K.; Voth, G. A.; Salvador, P.; Dannenberg, J. J. ; Zakrzewski, V. G. ; Dapprich, S. ; Daniels, A. D.; Strain, M. C.; Farkas, O.; Malick, D. K.; Rabuck, A. D.; Raghavachari, K.; Foresman, J. B.; Ortiz, J. V.; Cui, Q.; Baboul, A. G.; Clifford, S.; Cioslowski, J.; Stefanov, B. B.; Liu, G.; Liashenko, A.; Piskorz, P.; Komaromi, I.; Martin, R. L.; Fox, D. J.; Keith, T.; Al-Laham, M. A.; Peng, C. Y.; Nanayakkara, A.; Challacombe, M.; Gill, P. M. W. ; Johnson, B.; Chen, W.; Wong, M. W.; Gonzalez, C.; Pople, J. A. *Gaussian 03*, revision C.02; Gaussian, Inc.: Wallingford, CT, 2004.
(30) Hirschfelder, J. O.; Wigner, E. *J. Chem. Phys.* **1939**, *7*, 616–628.
(31) Skodje, R. T.; Truhlar, D. G.; Garrett, B. C. *J. Phys. Chem.* **1981**, *85*, 3019–3023.
(32) Coote, M. L.; Collins, M. A.; Radom, L. *Mol. Phys.* **2003**, *101*, 1329–1338.
(33) Corchado, J. C.; Chuang, Y. Y.; Fast, P. L.; Hu, W. P.; Liu, Y. P.; Lynch, G. C.; Nguyen, K. A.; Jackels, C. F.; Ramos, A. F.; Ellingson, B. A.; Lynch, B. J.; Melissas, V. S.; Villà J.; Rossi, I.; Coitiño, E. L.; Pu, J.; Albu, T. V.; Steckler, R.; Garrett, B. C.; Isaacson, A. D.; Truhlar, D. G. *POLYRATE*, version 9.7; University of Minnesota: Minneapolis, MN, 2007.
(34) Corchado, J. C.; Chuang, Y. Y.; Coitiño, E. L.; Truhlar, D. G. *GAUSSRATE*, version 9.7; University of Minnesota: Minneapolis, MN, 2007.
(35) Malick, D. K.; Petersson, G. A.; Montgomery, J. A., Jr. *J. Chem. Phys.* **1998**, *108*, 5704–5713.
(36) Saeys, M.; Reyniers, M. F.; Marin, G. B.; Van Speybroeck, V.; Waroquier, M. *J. Phys. Chem. A* **2003**, *107*, 9147–9159.
(37) Page, M.; McIver, J. W., Jr. *J. Chem. Phys.* **1988**, *88*, 922–935.
(38) Chuang, Y. Y.; Corchado, J. C.; Truhlar, D. G. *J. Phys. Chem. A* **1999**, *103*, 1140–1149.
(39) Villà, J.; Truhlar, D. G. *Theor. Chem. Acc.* **1997**, *97*, 317–323.
(40) Mcquarrie, D. A. *Statistical Mechanics*; University Science Books, 2000.
(41) Sumathi, R.; Carstensen, H. H.; Green, W. H., Jr. *J. Phys. Chem. A* **2001**, *105*, 6910–6925.
(42) Andersson, M. P.; Uvdal, P. *J. Phys. Chem. A* **2005**, *109*, 2937–2941.
(43) Chase, M. W., Jr. *J. Phys. Chem. Ref. Data* **1998**, Monograph 9.
(44) Feller, D.; Dixon, D. A.; Francisco, J. S. *J. Phys. Chem. A* **2003**, *107*, 1604–1617.
(45) Torrent-Sucarrat, M.; Anglada, J. M. *ChemPhysChem* **2004**, *5*, 183–191.
(46) Boys, S. F.; Bernardi, F. *Mol. Phys.* **1970**, *19*, 553–566.
(47) Ghigo, G.; Tonachini, G. *J. Chem. Phys.* **1999**, *110*, 7298–7304.
(48) Lynch, B. J.; Truhlar, D. G. *J. Phys. Chem. A* **2001**, *105*, 2936–2941.
(49) Coote, M. L. *J. Phys. Chem. A* **2004**, *108*, 3865–3872.

(50) Uchimaru, T.; Chandra, A. K.; Tsuzuki, S.; Sugie, M.; Sekiya, A. *J. Comput. Chem.* **2003**, *24*, 1538–1548.
(51) Melissas, V. S.; Truhlar, D. G. *J. Phys. Chem.* **1994**, *98*, 875–886.
(52) Chuang, Y. Y.; Truhlar, D. G. *J. Phys. Chem. A* **1997**, *101*, 3808–3814.
(53) Jayatilaka, D.; Lee, T. J. *J. Chem. Phys.* **1993**, *98*, 9734–9747.
(54) Rienstra-Kiracofe, J. C.; Allen, W. D.; Schaefer, H. F., III *J. Phys. Chem. A* **2000**, *104*, 9823–9840.
(55) Corchado, J. C.; Truhlar, D. G.; Espinosa-García, J. *J. Chem. Phys.* **2000**, *112*, 9375–9389.

JP802017Q